Novel semiconductor-laser-integrated active AFM optical probe with ultrashort pulses and nanoscale aperture

Fei-Hung Chu, Gennady A. Smolyakov, Kevin J. Malloy, and Alexander A. Ukhanov*
Actoprobe LLC, 800 Bradbury SE, Suite 160, Albuquerque, NM 87106

ABSTRACT

Optical characterization at the nanoscale currently requires instruments such as NSOM/TERS, or hybrid AFM with specialized far-field optical microscopes that are quite complicated and do not provide any time-resolved data. We have demonstrated a novel class of probes for Scanning Probe Microscopy (SPM) - an Ultrafast Pulsed Atomic Force Microscopy Optical Probe (UFP AAOP) that will enhance characterization capabilities at the nanoscale and provide an exciting opportunity for obtaining both space- and time-resolved chemical information simultaneously.

In the UFP AAOP design, a two-section quantum-dot mode-locked laser is monolithically integrated with an SPM probe fabricated from GaAs, with a nanoscale opening at the apex of the tip as the output aperture. With UFP AAOP, the light is supplied through the tip; hence, there is no scattered far-field light and thus significantly reduced background. Furthermore, the difficulties associated with laser alignment onto the tip and with imaging the signal onto a detector are avoided with the UFP AAOP. The UFP AAOP provides pulses with less than 4 ps duration and spatial resolution better than 300 nm at 1240 nm wavelength. It is potentially possible to reduce the pulse width to ~ 0.3 ps and to improve lateral resolution to ~ 0.5 nm. These unique optical probes will perform the functions of conventional AFM probes and simultaneously provide information about chemical properties of the sample at the nanoscale together with time-resolved spectroscopy. UFP AAOP will facilitate the creation of a new microscopy/spectroscopy instrument with combined single-molecule spatial resolution and ultrafast time-resolved capability.

Keywords: TERS, near field, AFM, confocal Raman spectroscopy, AFM active optical probe, NSOM.

1. INTRODUCTION

In the past 30 years, the Raman scattering technique has been established as the most sensitive probe of chemical composition, with many advances demonstrated in the development of spontaneous Raman (the most widely used, conventional type of Raman), surface-enhanced, and nonlinear Raman techniques. There has been significant progress in ultrafast nonlinear stimulated Raman spectroscopy (SRS) using ultrashort laser pulses [1], [2]. While SRS is a useful technique for observing molecular dynamics, it is very limited in terms of chemical specificity. The narrow-band pump and Stokes excitation fields interact with a single molecular vibration, and the overlapping Raman bands cannot be distinguished. Very often, a priori knowledge of the chemical content and specific molecular vibration spectrum is required to distinguish the overlapping Raman bands. Spontaneous Raman spectroscopy, on the other hand, offers a much more distinct fingerprint for convenient chemical identification, but is much less advanced in terms of ultrafast pulsed spectroscopy that provides information on ultrafast molecular dynamics. In the context of conventional spontaneous Raman, ultrafast pulsed spectroscopy is normally employed for fluorescence background rejection, based on different time scales for the fluorescence and Raman scattering processes [3], [4]. The very first attempts have recently been reported at making ultrafast spectroscopy with TERS [5], [6]. Demonstrating TERS with a pulsed excitation source is considered to be a very important step toward monitoring chemical reactions on the pico- to femtosecond time scale with the high spatial resolution and chemical specificity inherent with TERS. Integration of an external pulsed excitation source (typically a Ti:sapphire laser) is very challenging [6].

Attempts to integrate AFM and optical techniques have been made, but no products have been successfully introduced to customers. For example, AFM tips with integrated waveguides (hollow tips) have been used in conjunction with an external laser source [7], but this high-cost approach suffers from inherent limitations on optical resolution and delivered light power. For high lateral resolution, the size of the near-field aperture must be reduced, leading to an

*aukhanov@actoprobe.com; phone 1 703 946 5316; www.actoprobe.com

exponential decrease of optical power output. This approach has limited application to near-field microscopy, with an ultimate resolution of about 50 nm, but is not appropriate for optical spectroscopy because of the resultant low power output.

Other approaches aimed at better integration of light source and AFM tip have generally involved either a) attaching a prefabricated light source (edge emitter, VCSEL, or LED) above a Si AFM cantilever probe (hybrid approach) [8] or b) fabrication of the light source directly on the AFM tip [9]. In these instances, the optical detectors were not integrated into the probes. The hybrid approach has only been shown to work in research labs. Cost-effective fabrication of those optical probes to make them affordable for a wider scientific community is problematic because of the high cost and complexity of hybridization process. As for the approach used in [9], VCSELs, commonly used in this approach, are limited in their optical output power to less than 1 mW, which makes them useless for spectroscopy applications, especially for TERS.

Lastly, an AFM tip with integrated LED light source and photodetector has been demonstrated [10]. While the photodetector was monolithically fabricated into the probe, the light source (a GaAs LED) was simply glued onto the cantilever chip. This is insufficient to fulfill the requirement of high-power, single-wavelength operation, important for TERS, because LEDs have very broad emission spectrum not suitable for Raman excitation.

All the described approaches lack the necessary conditions for achieving efficient and affordable TERS, namely, a high-power single-line laser excitation source and a near-field photodetector monolithically integrated on the same AFM probe. To meet all these requirements, Actoprobe has designed and fabricated a monolithically integrated optical AFM probe [11-14] from commercially available GaAs-based semiconductor diode laser wafers. This approach of monolithic integration avoids very complicated and costly hybridization and should allow for high-volume manufacturing, resulting in a cost-effective, affordable product that can be adopted for use by all current AFM owners. The simplicity of this approach allows this technology to combine both single-molecule spatial resolution and ultrafast time resolution for pulsed TERS measurements. Ultrafast light pulses generated in the near field within a few nanometers distance of the tip will be free of any distortion normally associated with pulse propagation through focusing optics, and thus there will be no need for chirp compensation. The technology of mode-locked semiconductor lasers for ultrafast optical pulse generation is very well-established for various gain media. The best results in terms of pulse duration have been obtained from QD semiconductor lasers [15]. Pulses as short as 390 fs have been reported in two-section passively mode-locked QD lasers [16].

Besides being able to accomplish ultrafast pulsed TERS, the UFP AAOP technology can be modified to realize SRS or ultrafast pump-probe spectroscopy techniques [17]. The tip-enhanced capability of UFP AAOP will allow single-molecule resolution, currently not attainable with SRS [2] or confocal ultrafast pump-probe spectroscopy [18].

2. DEVELOPMENT OF UFP AAOP

The UFP AAOP technology naturally provides the ultrafast time-resolved spectroscopy capability that is integral to its design. The monolithically integrated semiconductor laser sources with specialized gain media, such as InAs quantum dots, offer mode-locking capabilities for sub-picosecond pulse generation. Integrating the ultrafast pulsed laser source into the GaAs AFM probe will allow probing the site-specific dynamic response of chemical systems. This imaging technique can be applied for exploring energy flow, molecular dynamics, breakage/formation of chemical bonds or conformational changes in nanoscale systems with combined molecular-scale spatial resolution and ultrafast time resolution not achievable in commercially available instruments. In this section, the designs of individual parts of the UFP AAOP are presented, with design considerations and parameters discussed.

2.1 Epitaxial laser structure with 5 QD layers

According to our analysis, epitaxial laser structures with 5 quantum-dot-in-a-well (QDWELL) [19-22] active layers have been found to be the most suitable for design and fabrication of semiconductor lasers with improved vertical divergence. The standard 1.3-µm epitaxial laser structure with 5 QDWELL active layers was grown by Innolume Gmbh. The layer structure specification and the results of photoluminescence characterization of the wafer are shown in Table 1 and in Fig. 1.

Product:	DO4892								
Layer	Material	Group	Repeat	Mole fraction (x		Thickness	Doping profile		Type	Dopant
				start	finish	(nm)	start	finish		
25	GaAs					60	1e20		P	C
24	Al(x)Ga(1-x)As			0.7	0	10	1e19		P	C
23	Al(x)Ga(1-x)As			0.7		1900	0.5-3e18		P	C
18	Al(x)Ga(1-x)As			0.98	0.7	25	1e18		P	C
16	Al(x)Ga(1-x)As			0.98		50	5e17		P	C
14	Al(x)Ga(1-x)As			0	0.98	10	1e18		P	C
13	GaAs					60			U/D	None
12	GaAs	1	5			40			U/D	None
11	In(x)Ga(1-x)As	1	5	0.15		3.5			U/D	None
10	InAs *	1	5			0.8			U/D	None
9	GaAs					100			U/D	None

Table 1. Layer structure specification.

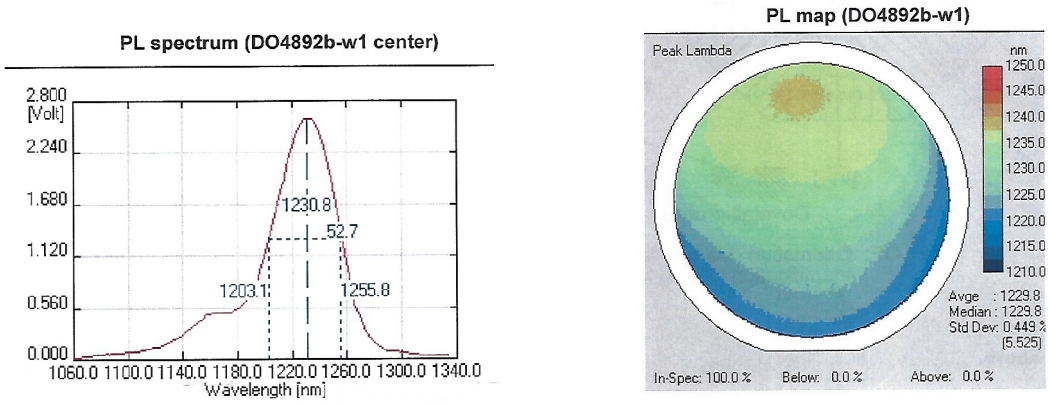

Fig. 1. Photoluminescence characterization of the laser wafer.

2.2 Three-section AAOP laser cavity design

The three-section mode-locked quantum dot laser design is illustrated in Fig. 2. It consists of a gain section, an absorber section, and an integrated photodetector (PD) section. The design parameters are based on similar structure used in [23], where a repetition rate of 7.4 GHz and pulses of 17 ps were achieved with the length of the gain section, L_g, of 4.73 mm, and the length of the absorber section, L_a, of 0.85 mm with two layers of QDs in the active region. Due to the limitations imposed by the probe geometry, the overall length of our device is shorter than that in [23], and the lengths L_a and L_g need to be rescaled accordingly considering also the number of QD layers to achieve similar performance. Since our epitaxial structure has five layers of QDs, we can make the absorption section 2.5 times shorter (L_a = 0.34 mm) to keep αL_a product the same, i.e., the same transmission for the absorption layer which controls the pulse width. We can also reduce the gain section 2.5 times to keep gL_g product the same, but we will not get the pulses of the same amplitude as in [23] for two reasons. First, the pulse repetition rate increases for shorter devices, and the gain has less time between the pulses to restore to its unsaturated value, hence the maximum achievable gain in the gain section will be smaller. Second, shorter devices have higher distributed mirror losses, and more gain is required to compensate for that too. Therefore, higher current density would be necessary to get the pulses of comparable amplitude to those obtained in [23].

There is a danger that QD gain might saturate below the value required to reach the lasing threshold. The mode-locking would still be possible but with pulses of low amplitude. So, when deciding on the lengths of the sections, we went in favor of the gain section, and divided the total 3.5 mm length as L_a = 0.34 mm, and L_g = 3.16 mm.

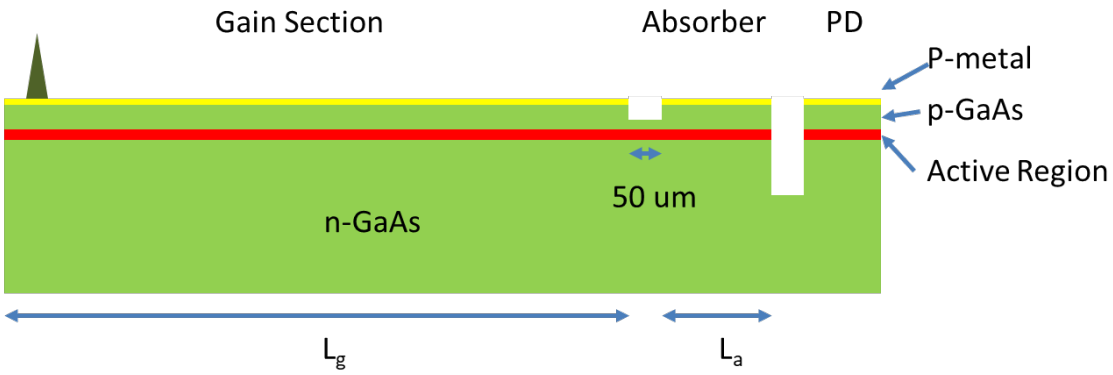

Fig. 2. Three-section mode-locked QD laser with integrated photodetector.

2.3 Folding mirror design and fabrication

In order to direct the output from the laser cavity into the tip, which is perpendicular to the laser cavity, a mechanism is required. The simplest design is a 45-degree folding mirror for vertical output, where a slope is etched right next to the output mirror of the laser as illustrated in Fig. 3. The folding mirror can be etched with angled dry etching or with focused-ion-beam (FIB) milling.

Fig. 4 shows the fabricated Fabry-Perot test structure of the folding mirror. The 45° folding mirror is milled with FIB. An almost circular and symmetrical optical output is observed with the infrared camera indicating the output is almost perpendicular to the surface, which is also confirmed with an infrared viewing card. The threshold current of this laser is around 90 mA as seen from the L-I curve in Fig. 5. The effectiveness of the folding mirror can be improved by reducing the roughness of the folding mirror and/or coating the mirror with metal. To reduce the roughness, a fine-tuned FIB procedure, as well as a well-calibrated dry etching procedure, can be used.

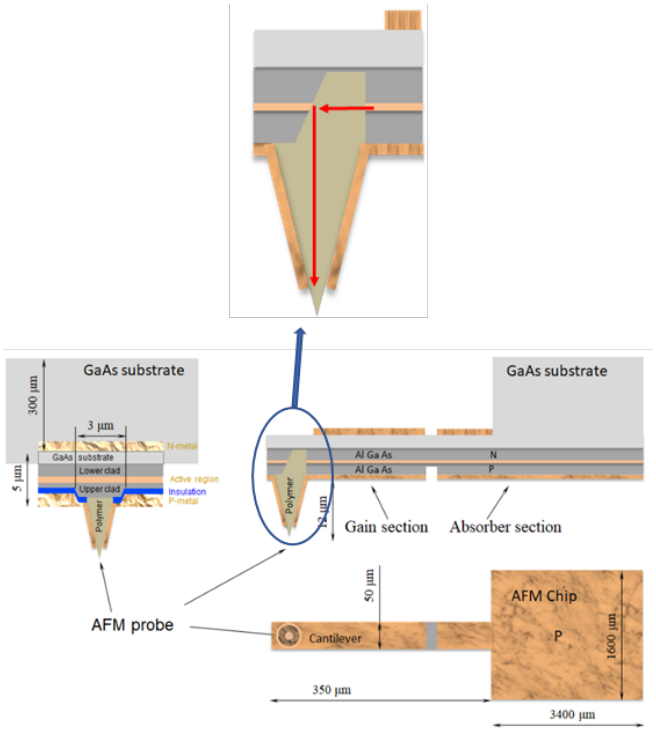

Fig. 3. UFP AAOP design: cross-sectional view, side view, bottom view, and magnified view of the tip.

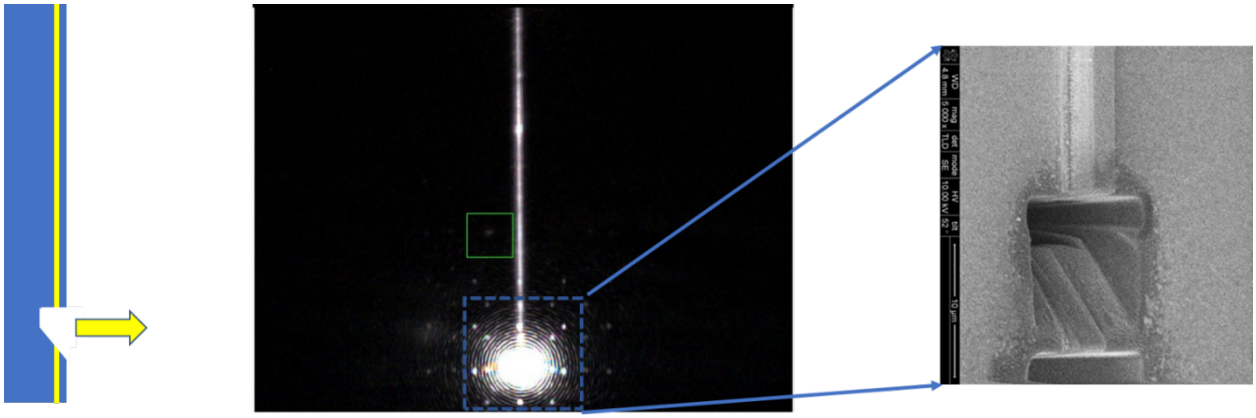

Fig. 4. Schematic of the structure (left), image from the camera (middle), and SEM image of the waveguide.

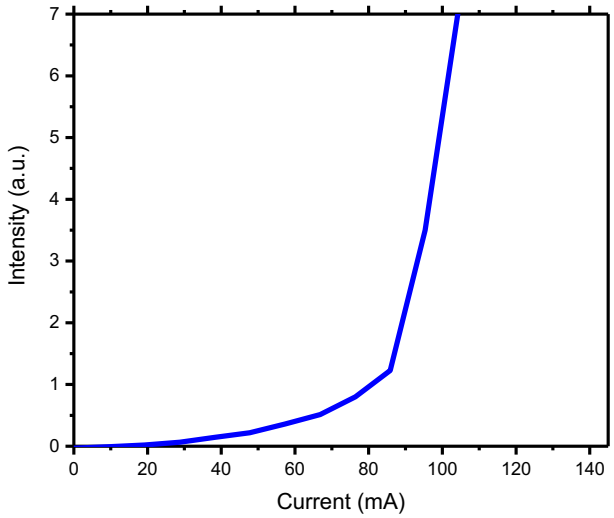

Fig. 5. L-I curve of the structure in Fig. 4.

2.4 Polymer tip design and fabrication

The simplest way to make polymer tips is by exposing and developing thick photoresists with suitable patterns. The thickest photoresist that we had available was AZ9260. Fig. 6 shows the spin curve of AZ9260 on a 6-inch silicon wafer [24]. A thickness around 10 µm was achieved at 2000 rpm. Thicker films were attainable at lower spin speeds but resulted in larger area of edge beads and more nonuniform film.

To fabricate the tips, the photoresist was spun at 2000 rpm followed by a 5-minute softbake. The pattern was then exposed for 30 seconds and developed in AZ421 developer until the photoresist on the exposed areas was completely removed. Some of the results from square and circular patterns are shown in the SEM images in Fig. 7 and Fig. 8, respectively. Square patterns resulted in sharper tips compared to circular patterns. The optimal sizes were somewhere from 6 µm to 10 µm.

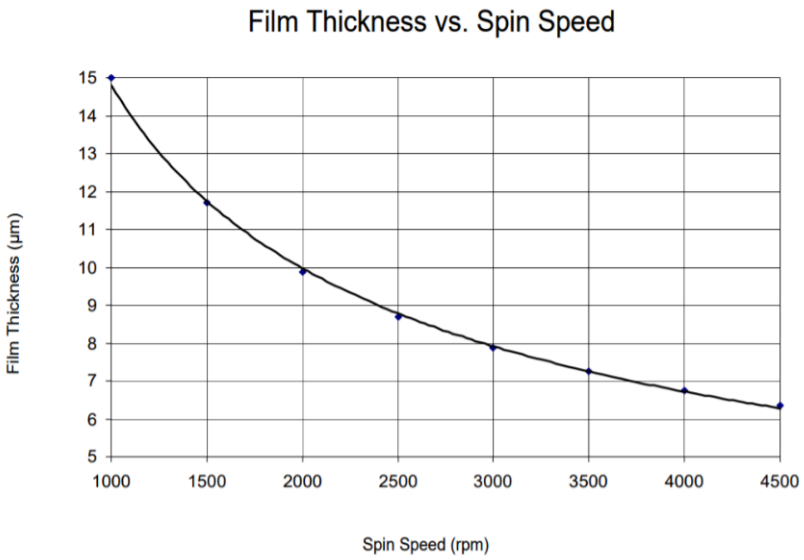

Fig. 6. Spin curve of AZ 9260 on a 6-inch silicon wafer [24].

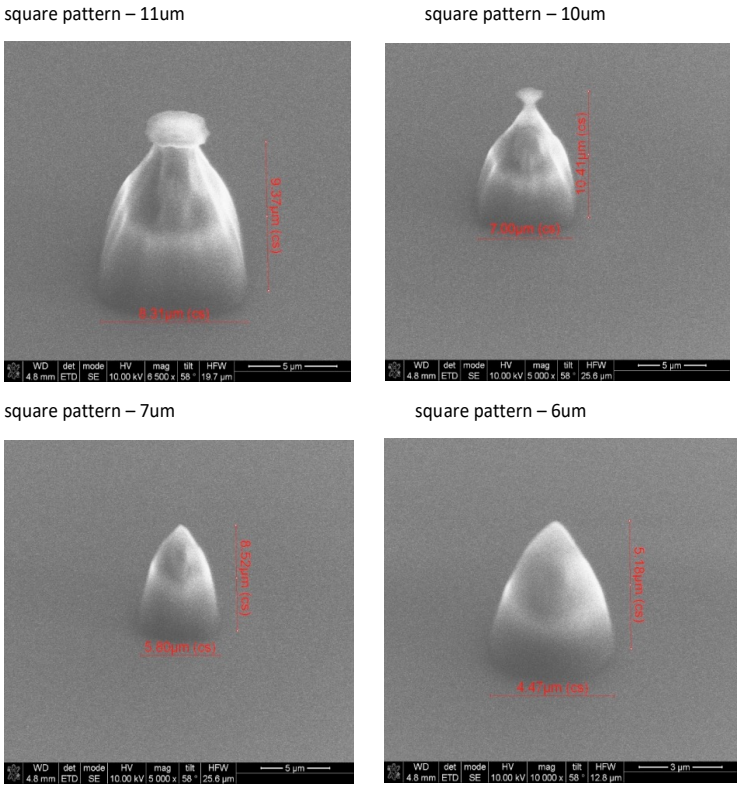

Fig. 7. Polymer tips formed from square patterns.

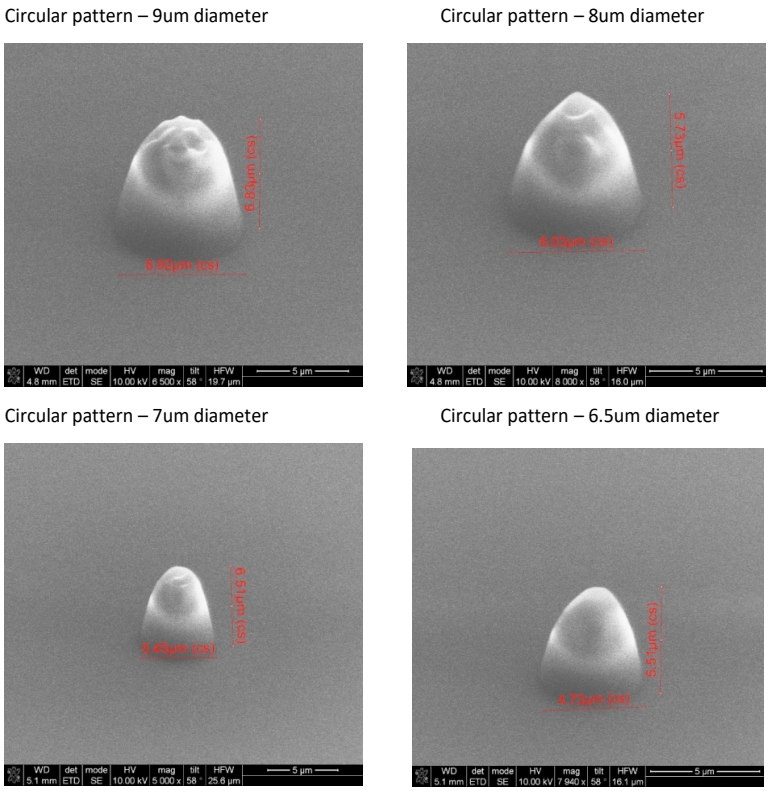

Fig. 8. Polymer tips formed from circular patterns.

3. UFP AAOP TESTING

3.1 Probe tip testing in AFM system

Fig. 9 shows the SEM image of the fabricated probes integrated with ridge waveguide before separation into individual AAOP devices. Also shown are the zoomed-in images of the cantilever and the polymer tip. The cantilevers have thicknesses ranging from 30 µm to 100 µm due to non-uniform material removal during the wet-etching process. The folding mirror is positioned behind the tip and the height of the tip is approximately 6 µm. A thin gold coating with a thickness of 75 nm is deposited on top of the tip with a circular opening of ~0.3 µm in diameter at the apex of the tip as the output aperture. Fig. 10 shows a finite-difference time-domain simulation of the optical near-field output from the aperture. The near-field optical resolution ~ 20 nm can be achieved by further reducing the aperture size in this passive optical probe design and with active optical probe design it can be reduced to less than 1 nm.

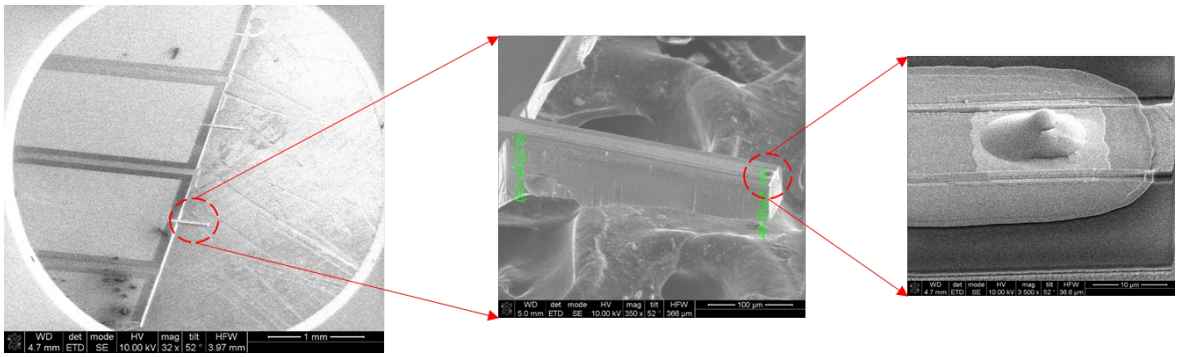

Fig. 9. SEM image of a fabricated device before separation (left) with zoomed-in images on the cantilever (middle) and the polymer tip (right).

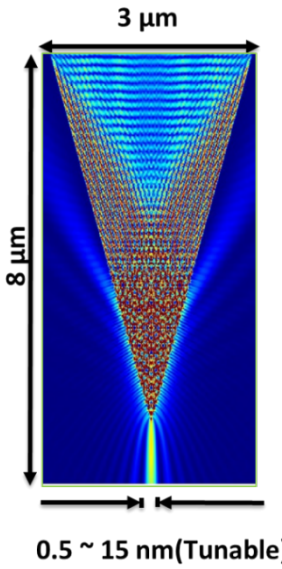

Fig. 10. FDTD simulation of laser light coupling into the optical near field at the AFM probe apex.

The L-I curve (Fig. 11c) was measured to determine the threshold current of the AAOP with a duty cycle of 6% under 100-Hz modulation frequency. The threshold current of the device being tested was ~180 mA. When using a higher magnification (20X) objective, a bright output can be seen from the tip (Fig. 11b). In order to mount the AAOP on the AFM, the probe holder was modified to allow biasing without crushing the waveguide. The device was mounted in the AFM system in tapping mode. The resonance frequency of the probes varied from below 100 kHz to 400 kHz due to variation in thickness. The AAOP being tested had a resonance frequency of 488 kHz (Fig. 11d).

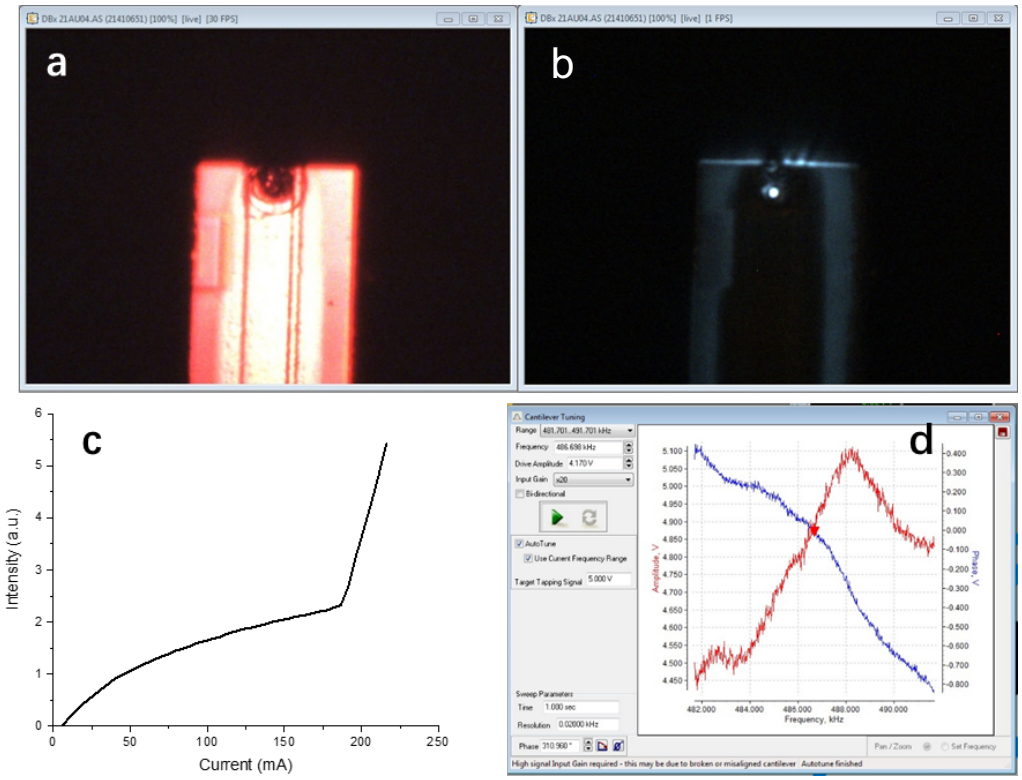

Fig. 11. (a) and (b) are the optical image of the tip; (c) is the L-I curve of the tip laser, and (d) is the tuning frequency of the tip.

Fig. 12 shows a comparison of the AFM scans on a calibration sample with 10-µm pitch between a commercial Si probe and our AAOP with a polymer tip, verifying the AFM scanning capability of the fabricated AAOP. The slightly distorted image in the middle of the square patterns is due to the large radius of curvature at the apex of the tip that can be improved by calibrating the tip fabrication process.

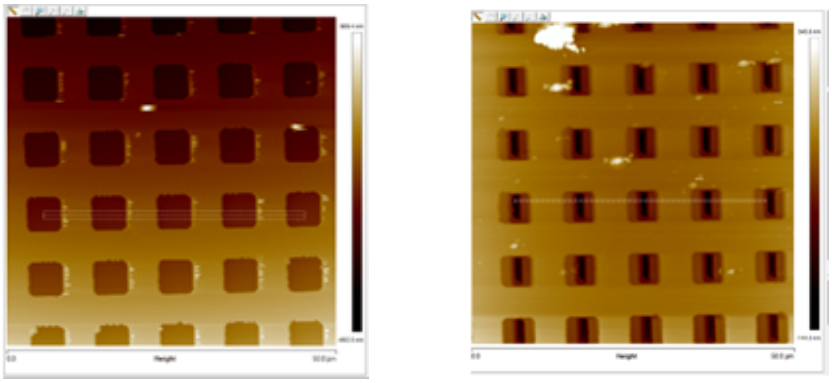

Fig. 12. AFM scan on a 10-µm pitch calibration sample using commercial Si probe (left) and AAOP with polymer tip (right).

To use the AAOP sub-micron optical source for near-field optical scanning, the laser can be biased at a current suitable for a specific application. In Fig. 13 a near-field optical scan was done with the laser biased slightly above threshold at 215 mA. The optical image was collected through an objective when the AFM scanned across the sample. It shows high correlation with the AFM image. In this near-field optical image we can observe light shift from the holes centers of the calibration sample which is typical for NSOM images on such type of objects.

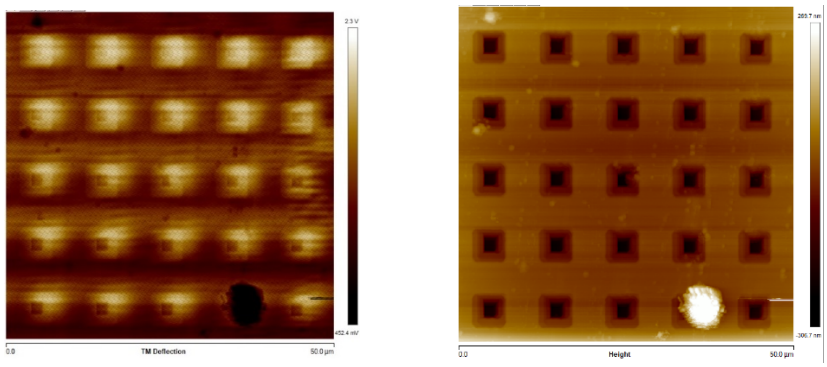

Fig. 13. Near-field optical image (left) using AAOP with polymer tip, and AFM image (right) on a 10-µm-pitch calibration sample.

3.2 UFP AAOP testing

To demonstrate the feasibility of the UFP AAOP for time-resolved spectroscopy, we purchased a two-section mode-locked QD laser (Fig. 14) with a structure similar to our design. The QD laser was manufactured by Innolume GmbH, the same foundry that provides us with epitaxy growth service. The QD laser was packaged in a fiber-coupled butterfly package to facilitate optical coupling and measurement. A customized temperature controlled laser driver was used to drive the laser gain and absorber sections. Under mode-locking condition, the laser produced pulses shorter than 4 ps with a repetition rate of ~11.37 GHz as shown in the RF- power spectrum and autocorrelator measurement in Fig. 15.

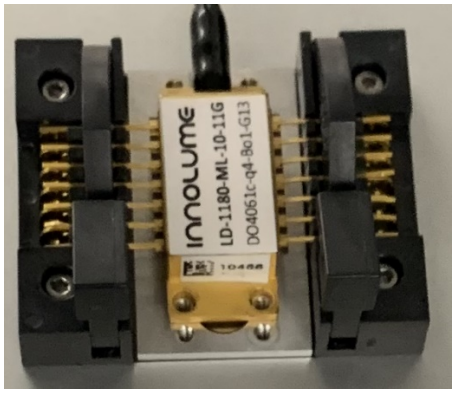

Fig. 14. Commercial mode-locked QD laser in fiber-coupled butterfly package from Innolume Gmbh with the epitaxial and waveguide structures similar to those of our AAOP device.

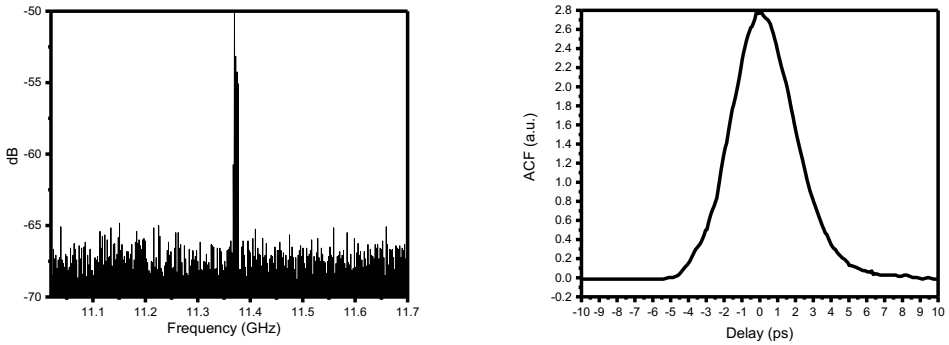

Fig. 15. The microwave power spectrum (left) and autocorrelator measurement of the pulse shape (right) showing 11.37 GHz repetition rate and ~ 4 ps pulse width under the optimum bias condition of I_g = 100 mA and V_a = 10 V from the commercial mode-locked QD laser.

A two-section AAOP device, designed for ultra-fast-pulsed mode-locked operation, with 5-µm-wide ridge-waveguide laser, 380-µm-long absorber section, and 3360-µm-long gain section is shown in Fig. 16. The wavelength of the AAOP was λ = 1240 nm while that for the commercial laser was λ = 1180 nm. The L-I curves of the commercial QD laser and the AAOP for various reverse bias on the absorber section are presented in Fig. 17 demonstrating the effectiveness of the absorbers in both devices. The optical spectra, also shown in Fig. 17, verify the ground-state emission when the devices were under mode-locking conditions and the large change of the spectral shape during mode-locking as compared to CW operation. From the similarities observed in L-I curves and optical spectra of the two devices, we conclude that the AAOP was mode-locked with pulse characteristics similar to those shown in Fig. 15. Fig. 18 shows a two-section AAOP device integrated into a customized AFM probe holder that fits a standard AFM.

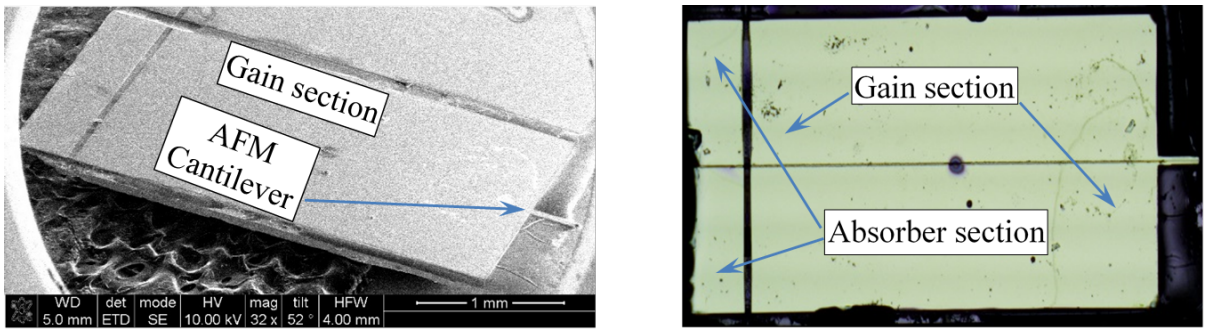

Fig. 16. SEM image (left) and optical image (right) of a two-section AAOP device.

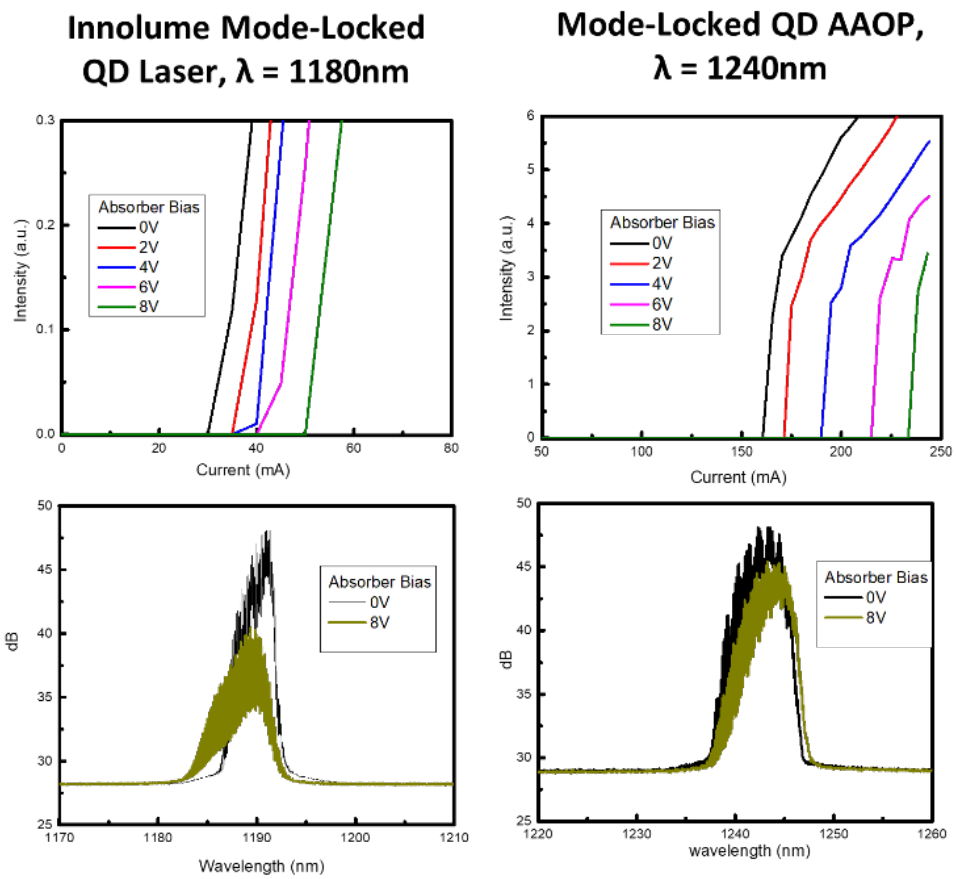

Fig. 17. L-I curves (top) and optical spectra (bottom) under various absorber bias conditions of the commercial mode-locked QD laser (left) and UFP AAOP (right).

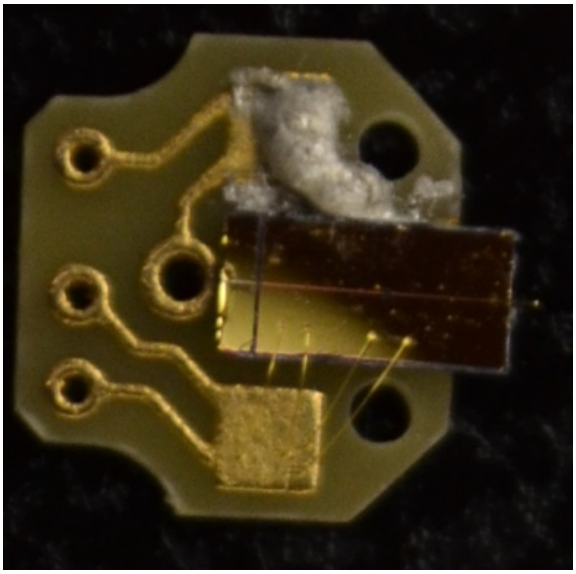

Fig. 18. A two-section AAOP device integrated into a customized AFM probe holder.

4. NOVEL CONCEPT OF INTEGRATED III-V/SILICON AAOP

Actoprobe LLC has been pursuing the concept of AAOP fabricated entirely from GaAs-based or similar semiconductor laser materials, including the semiconductor laser source, the cantilever with the tip on its end, and the probe base, all monolithically integrated into a semiconductor chip for combined AFM/NSOM/TERS measurements. As important as it is for establishing the general concept of AAOP, this approach is not economical in utilizing relatively expensive III/V material, which makes the final product rather costly. At the same time, in terms of their mechanical properties, GaAs-based cantilever AFM probes are typically inferior to standard silicon cantilever AFM probes. To take full advantage of both the III/V semiconductor laser technology and the established silicon microfabrication techniques of the standard technology of AFM tip/cantilever manufacturing, we propose a novel concept of integrated III-V/silicon AAOP.

The innovation is accomplished by integrating a III-V semiconductor laser source into a silicon cantilever AFM probe. As before, we propose a special intracavity design for the AAOP where the gold-coated silicon tip itself acts also as the output laser mirror. In that way, the probe tip is part of the laser cavity that is immediately supplied with intracavity high-intensity laser light. This design takes advantage of the high-intensity intracavity laser light supplied through the tip and delivered directly to the tip apex.

We have found a promising III-V silicon integration approach, developed by Skorpios Technologies [25]. The approach is based on metal bonding the III-V gain medium section to the SOI silicon substrate for direct optical coupling (edge- or butt coupling) between the III-V gain section and the silicon layer of the SOI waveguide. As distinct from other configurations, the III-V gain section is planar with the silicon waveguide layer, providing high efficiency optical coupling.

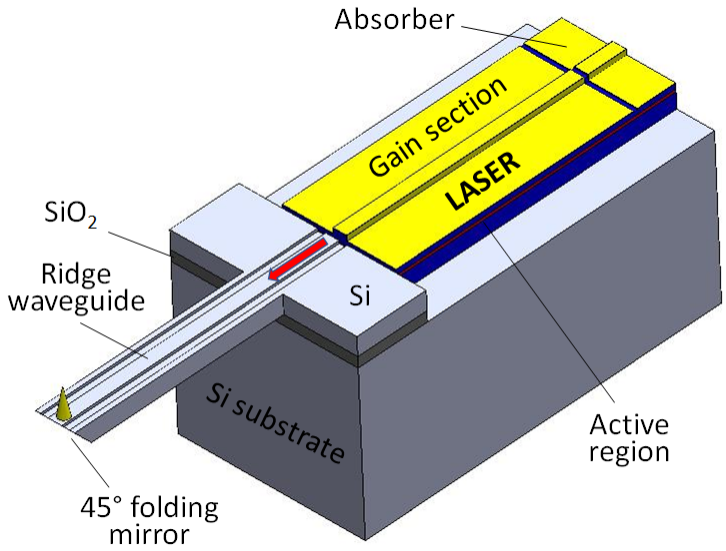

Fig. 19. Illustration of integrated III-V/silicon AAOP concept.

The concept of integrated III-V/silicon AFM active optical probe is shown in Fig. 19. The base of the probe, the cantilever, the tip, and the SOI ridge waveguide are structured in the first stage of fabrication process from a special SOI wafer. The silicon waveguide layer is sufficiently thick (~10 μm) to allow fabrication of a tip sitting on top of a relatively thick (~ 5 μm) silicon ridge waveguide extending from the probe base to the cantilever. An epitaxial III-V gain material is embedded in the base of the probe in such a way that its active layer is planar and properly aligned with the silicon ridge waveguide to efficiently couple the laser light into the ridge waveguide by way of butt (edge) coupling. The epitaxial III-V gain material piece is metal-bonded to the silicon substrate within the pre-etched pit receptor site inside the base of the probe and then processed into the laser chip. The light is delivered to the end of the cantilever where it is redirected vertically from the silicon waveguide into the probe tip using a folding mirror. The gold-coated tip acts as an output laser mirror

(total internal reflection conical prism) in the special intracavity design of the AAOP. The light reflected from the gold-coated tip is coupled back into the silicon waveguide and, eventually in the laser chip active region. This light feedback mechanism has to be sufficiently strong to make sure that the probe tip is supplied with intracavity high-intensity laser light. One of the main advantage of this approach is good thermal conductivity through the silicon substrate.

As proof-of-principle, we propose to make a first prototype of the integrated III-V/silicon AAOP by integrating a III-V semiconductor laser chip into a commercially available silicon cantilever AFM probe. In this approach, a III-V semiconductor laser chip is buried in the base of a commercially available silicon AFM probe in front of the cantilever and aligned with the cantilever to efficiently couple the laser light into the cantilever by way of butt (edge) coupling (Fig. 20). An epitaxial III-V gain material piece is metal-bonded within pre-etched pit receptor site inside the base of the silicon AFM probe and then processed into the laser chip. The cantilever acts as an optical waveguide with silicon core and air claddings.

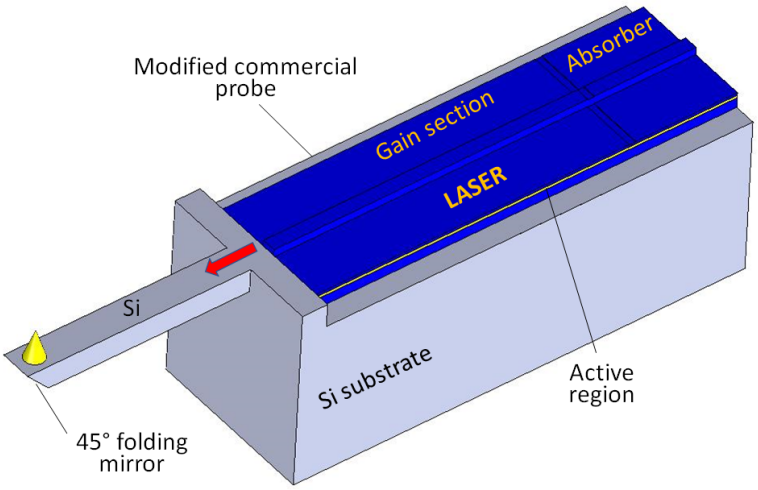

Fig. 20. Integrated III-V/silicon AAOP based on a commercial silicon cantilever AFM probe.

So far, an even simpler concept of integrated III-V/silicon AAOP with free-space illumination of the probe tip has been demonstrated. The concept is based on integrating a semiconductor laser source into a cantilevered silicon AFM probe in such a way that the free propagating light from the integrated laser source can be used to illuminate the probe tip and carry out AFM, NSOM, and TERS measurements. A semiconductor laser chip was bonded directly to the top surface of the base of a commercial AFM probe without any prior probe modification (no pit receptor site etching into the base of the probe). The active region of the laser chip was aligned with the probe tip, so that the free propagating light from the integrated laser source was used to illuminate the probe tip and carry out AFM and NSOM measurements.

Fig. 21 shows an example of a silicon-integrated AFM active optical probe. Using lithography and ICP dry etching, a standard silicon AFM probe was patterned and etched to a depth of 150 μm to accommodate a thick photonic crystal laser chip with improved vertical divergence [26]. Fig. 21 shows the laser chip bonded to the silicon probe with indium. The top view shows the laser light at the output facet of the laser and scattered light at the tip. Fig. 22 shows the optical spectrum of the silicon-integrated laser source, measured using the light scattered from the probe tip. The results of AFM and near-field optical testing of the silicon-integrated AFM active optical probe are presented in Fig. 23. Fig. 24 summarizes the results of experimental measurement of the laser beam divergence. The transverse size of the laser beam is measured directly on the laser output facet and 1.3 mm away from the output facet.

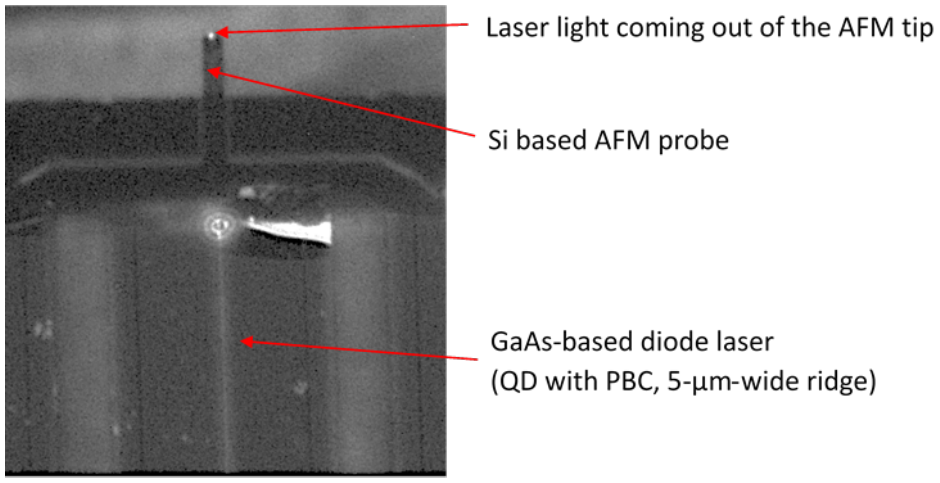

Fig. 21. Silicon-integrated active AFM optical probe with laser chip bonded to a silicon probe - top view.

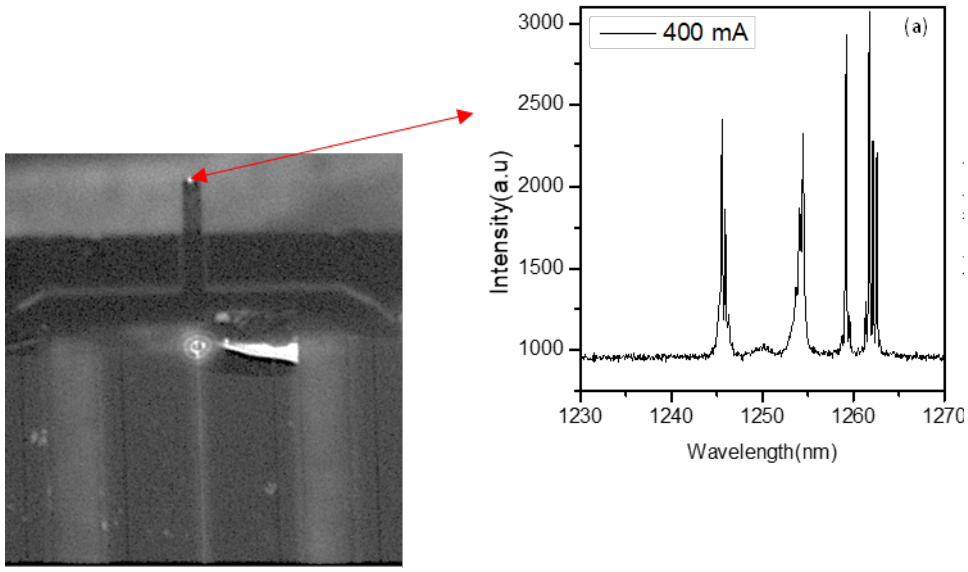

Fig. 22. Optical spectrum of the silicon-integrated laser source measured using the light scattered from the probe tip.

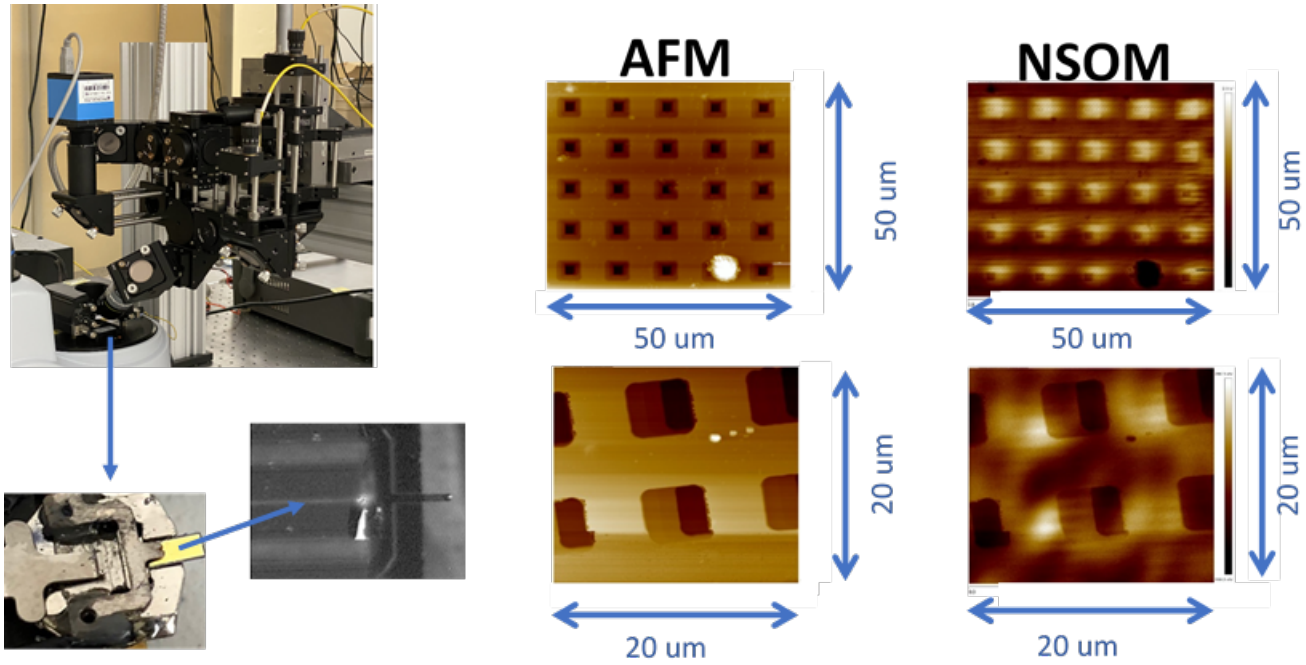

Fig. 23. Results of AFM and near-field optical testing of the silicon-integrated AFM active optical probe.

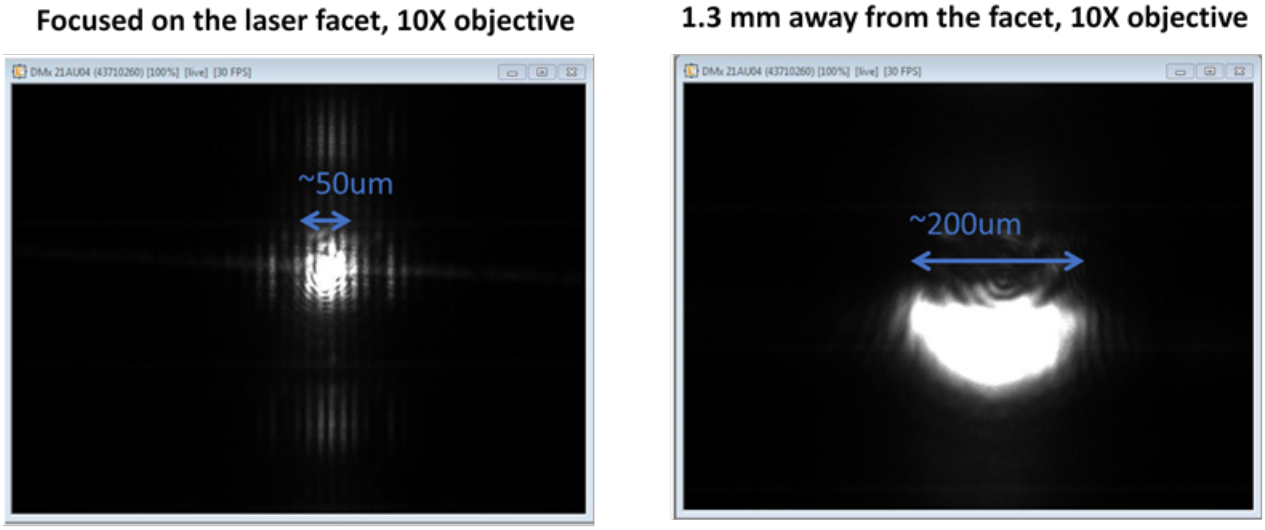

Fig. 24. Results of experimental measurement of the laser beam divergence.

5. CONCLUSIONS

We have demonstrated a novel type of AFM probe – Ultra-Fast AFM Active Optical Probe (UFP AAOP) by monolithically integrating a mode-locked diode laser and AFM tip. This novel optical AFM probe simultaneously focuses laser light in space and time and is capable of delivering significant amount of optical power to single-molecule scale, which is very attractive for non-linear optical spectroscopy and nanoscopy. The UFP AAOP capability of generating sub-picosecond optical pulses also makes it very attractive for single-molecule time-resolved spectroscopy. It can also be applied for THz

spectroscopy and quantum computing. Most importantly, it will make near-field optical microscopy and spectroscopy faster, more convenient, and affordable. Finally, we have proposed a novel concept of integrated III-V/silicon AAOP that takes full advantage of both the III/V semiconductor laser technology and the established silicon microfabrication techniques of the standard technology of AFM tip/cantilever manufacturing.

6. ACKNOWLEDGEMENTS

This work was supported by the Department of Energy Research Grant DE-SC0015188. The work was performed, in part, at the Center for Integrated Nanotechnologies, an Office of Science User Facility operated for the U.S. Department of Energy Office of Science by Los Alamos National Laboratory and Sandia National Laboratories. Actoprobe LLC team would like to thank the faculty and technical stuff of the Center for High Technology Materials (CHTM) at the University of New Mexico for fruitful discussions and technical support.

REFERENCES

[1] R. R. Frontiera, A. I. Henry, N. L. Gruenke, R. P. Van Duyne, "Surface-enhanced femtosecond stimulated Raman spectroscopy", J. Phys. Chem. Lett. 2(10), 1199-1203 (2011).
[2] A. A. Lanin, E. A. Stepanov, R. A. Tikhonov, et al., "Multimodal nonlinear Raman microspectroscopy with ultrashort chirped laser pulses", JETP Lett. 101(9), 593-597 (2015).
[3] N. Everall, T. Hahn, P. Matousek, et al., "Picosecond time-resolved Raman spectroscopy of solids: Capabilities and limitations for fluorescence rejection and the influence of diffuse reflectance", Appl. Spect. 55(12), 1701-1708 (2001).
[4] I. Nissinen, J. Nissinen, P. Keranen, et al., "A 2x(4)x128 multitime-gated SPAD line detector for pulsed Raman spectroscopy", IEEE Sens. J. 15(3), 1358-1365 (2015).
[5] J. M. Klingsporn, M. D. Sonntag, T. Seideman, R. P. Van Duyne, "Tip-enhanced Raman spectroscopy with picosecond pulses", J. Phys. Chem. Lett. 5(1), 106-110 (2014).
[6] M. D. Sonntag, E. A. Pozzi, N. Jiang, et al., "Recent advances in tip-enhanced Raman spectroscopy", J. Phys. Chem. Lett. 5(18), 3125-3130 (2014).
[7] M. Celebrano, P. Biagioni, M. Zavelani-Rossi, et al., "Hollow-pyramid based scanning near-field optical microscope coupled to femtosecond pulses: A tool for nonlinear optics at the nanoscale," Rev. Sci. Instr. 80(3), 033704 (2009).
[8] J. W. Kingsley, S. K. Ray, A. M. Adawi, et al., "Optical nanolithography using a scanning near-field probe with an integrated light source," Appl. Phys. Lett. 93(21), 213103 (2008).
[9] K. Hoshino, A. Gopal, and X. Zhang, "Near-field scanning nanophotonic microscopy – breaking the diffraction limit using integrated nano light-emitting probe tip," IEEE J. Select. Topics Quantum Electron. 15(5), 1393–1399 (2009).
[10] M. Sasaki, K. Tanaka, and K. Hane, "Scanning near-field optical microscope using cantilever integrated with light emitting diode, waveguide, aperture, and photodiode," in Optical MEMS, 2000 IEEE/LEOS International Conference on Optical MEMS, 129–130 (2000).
[11] T. J. Rotter, T. Busani, P. Rathi, F. Jaeckel, P. A. Reyes, K. J. Malloy, A. A. Ukhanov, E. Plis, S. Krishna, M. Jaime-Vasquez, N. F. Baril, J. D. Benson, D. A. Tenne, "Confocal Raman Spectroscopy and AFM for evaluation of sidewalls in type II super lattice FPAs", Proc. SPIE 9451, 94510R (2015).
[12] A. A. Ukhanov, G. A. Smolyakov, "Atomic force microscopy active optical probe", Patent No. US 9482691, issued November 01, 2016.
[13] F.-H. Chu, G. A Smolyakov, C. F. Wang, Y. Gao, C. Wang, K. J. Malloy, A. A. Ukhanov, D. V. Pete, M. Jaime-Vasquez, N. F. Baril, J. D. Benson, D. A. Tenne, "Tip-enhanced stimulated Raman scattering with ultra-high-aspect-ratio tips and confocal polarization Raman spectroscopy for evaluation of sidewalls in Type II superlattices FPAs", Proc. SPIE 10726, 107261C (2018).
[14] A. A. Ukhanov, G. A. Smolyakov, F. H. Chu, C. Wang, "Monolithic atomic force microscopy active optical probe", Patent No. US 11,016,119, issued May 25, 2021.
[15] E. U. Rafailov, M. A. Cataluna, W. Sibbett, "Mode-locked quantum-dot lasers", Nature Photonics 1, 395-401 (2007).
[16] E. U. Rafailov, M. A. Cataluna, W. Sibbett, et al., "High-power picosecond and femtosecond pulse generation from a two-section mode-locked quantum-dot laser", Appl. Phys. Lett. 87(8), 081107 (2005).
[17] X. L. Wang, H. Yokoyama, T. Shimizu, "Synchronized harmonic frequency mode-locking with laser diodes through optical pulse train injection", IEEE Photon. Tech. Lett. 8(5), 617-619 (1996).
[18] T. Virgili, G. Grancini, E. Molotokaite et al. "Confocal ultrafast pump-probe spectroscopy: a new technique to explore nanoscale composites", Nanoscale 4(7), 2219-2226 (2012).

[19] A. A. Ukhanov, R. H. Wang, T. J. Rotter, A. Stintz, L. F. Lester, P. G. Eliseev, K. J. Malloy, “Orientation dependence of the optical properties in InAs quantum-dash lasers on InP”, Appl. Phys. Lett. 81(6), 981-983 (2002).
[20] A. A. Ukhanov, A. Stintz, P. G. Eliseev, K. J. Malloy, “Comparison of the carrier induced refractive index, gain, and linewidth enhancement factor in quantum dot and quantum well lasers”, Appl. Phys. Lett. 84(7), 1058-1060 (2004).
[21] A. A. Ukhanov, A. S. Bracker, G. Boishin, J. C. Culbertson, “Multistep fabrication of self-assembled unstrained quantum dashes”, J. Vac. Sci. Technol. B 24(3), 1577-1580 (2006).
[22] A. A. Ukhanov,“Study of the carrier-induced optical properties in III-V quantum confined laser nanostructures”, Ph.D. dissertation, Univ. New Mexico, Albuquerque (2004).
[23] X. Huang, A. Stintz, H. Li, L. F. Lester, J. Cheng, and K. J. Malloy, “Passive mode-locking in 1.3 μm two-section InAs quantum dot lasers”, Appl. Phys. Lett. 78(19), 2825-2827 (2001).
[24] https://www.nanofab.utah.edu/svn/public/documents/Non%20SOPs/Photoresist/ az_9260_photoresist.pdf.
[25] T. Creazzo, E. Marchena, S. B. Krasulick, P. K. L. Yu, D. Van Orden, J. Y. Spann, C. C. Blivin, L. He, H. Cai, J. M. Dallesasse, R. J. Stone, and A. Mizrahi, "Integrated tunable CMOS laser," Opt. Express 21(23), 28048-28053 (2013).
[26] L. Liu, H. Qu, Y. Liu, Y. Zhang, Y. Wang, A. Qi, and W. Zheng, “High-power narrow-vertical-divergence photonic band crystal laser diodes with optimized epitaxial structure”, Appl. Phys. Lett. 105(23), 231110 (2014).